Fractal and Projected Structure Properties of Soot Aggregates

Ü. Ö. KÖYLÜ and G. M. FAETH*
Department of Aerospace Engineering, The University of Michigan, Ann Arbor, Michigan 48109-2118, U.S.A.

T. L. FARIAS and M. G. CARVALHO
Mechanical Engineering Department, Instituto Superior Técnico, 1096 Lisbon, Portugal

The structure of soot aggregates was investigated, emphasizing the fractal properties as well as the relationships between the properties of actual and projected soot images. This information was developed by considering numerically simulated soot aggregates based on cluster–cluster aggregation as well as measured soot aggregates based on thermophoretic sampling and analysis by transmission electron microscopy (TEM) of soot for a variety of fuels (acetylene, propylene, ethylene, and propane) and both laminar and turbulent diffusion flame conditions. It was found that soot aggregate fractal properties are relatively independent of fuel type and flame condition, yielding a fractal dimension of 1.82 and a fractal prefactor of 8.5, with experimental uncertainties (95% confidence) of 0.08 and 0.5, respectively. Relationships between the actual and projected structure properties of soot, e.g., between the number of primary particles and the projected area and between the radius of gyration of an aggregate and its projected image, also are relatively independent of fuel type and flame condition.

NOMENCLATURE

A_a	projected area of an aggregate
A_p	cross-sectional area of a primary particle, $\pi d_p^2/4$
d	burner diameter
d_p	diameter of primary particle
D_f	aggregate fractal dimension
k_a	projected area prefactor, Eq. 2
k_f	fractal prefactor based on R_g, Eq. 1
k_{fL}	fractal prefactor based on $(LW)^{1/2}$, Eq. 5
L	projected maximum length of aggregate
N	number of primary particles in an aggregate
$R_g, R_g(3D)$	radius of gyration of an aggregate
$R_g(2D)$	radius of gyration of projected aggregate image
W	maximum projected aggregate width normal to L
x	height above burner, coordinate direction
x_p	primary particle size parameter, $\pi d_p/\lambda$
y	coordinate direction
z	coordinate direction

Greek Symbols

α	projected area exponent
λ	wavelength of light

INTRODUCTION

Practical hydrocarbon fueled flames generally contain and emit soot, which affects their radiation, structure, and pollutant emission properties. These effects have motivated considerable interest in the structure and optical properties of soot, in order to develop nonintrusive methods for measuring soot properties and to estimate the continuum radiation and heterogeneous reaction properties of soot in flame environments. The present investigation seeks to contribute to a better understanding of soot structure, by undertaking a computational and experimental study of the structure of soot aggregates, emphasizing characteristics needed to define soot optical and fractal prop-

* Corresponding author.

COMBUSTION AND FLAME 100: 621–633 (1995)

Published by Elsevier Science Inc.

0010-2180/95/$9.50
SSDI 0010-2180(94)00147-K

erties, and to understand the relationships between actual and projected soot images.

Earlier work concerning the structure and optical properties of soot has been reviewed by Tien and Lee [1], Viskanta and Mengüc [2], Jullien and Botet [3], and Köylü and Faeth [4]; therefore, consideration of past studies will be brief. Initial studies of the structure of soot by Williams and coworkers [5–7] involved thermophoretic and molecular beam sampling of premixed acetylene, benzene and propane flames, followed by analysis using transmission electron microscopy (TEM). The results showed that soot consisted of small spherical primary particles, having nearly constant diameters, collected into open structured aggregates that had broad distributions of the number of primary particles per aggregate. Subsequent work using thermophoretic sampling and TEM established similar behavior for a variety of fuels and flame conditions, e.g., laminar and turbulent flames as well as premixed and diffusion flames [8–21]. In general, the distributions of primary particle diameters had standard deviations of 15%–25% of the mean primary particle diameter, supporting the observations of nearly uniform primary particle sizes [4]. Additionally, primary particle diameters generally were less than 60 nm, with the largest diameters associated with heavily sooting fuels [4]. This behavior yields primary particle size diameters, $x_p < 0.4$, for wavelengths of interest for optical measurements of soot properties and estimates of continuum radiation from soot ($\lambda > 500$ nm). As a result, it is reasonable to assume that individual primary particles approximate Rayleigh scattering particles, e.g., their total scattering and absorption cross-sections typically are within 1% and 5%, respectively, of estimates based on Mie scattering theory for $\lambda > 500$ nm [4].

Soot aggregates are small near the soot inception point in flames but they aggregate rapidly with the mean number of primary particles per aggregate reaching values in the range 200–600 for soot emitted from large buoyant turbulent diffusion flames [4]. As noted earlier, unlike primary particle diameters, aggregate size distributions are broad; in fact, the standard deviations of aggregate size are comparable to the mean value of the number of primary particles in an aggregate. Thus, aggregate size distributions generally are represented by the log normal size distribution function while 95% of the soot aggregates emitted from large turbulent diffusion flames contain 30–1800 primary particles [4, 19]. This complexity of aggregate size distributions, however, is mitigated by the observation that soot aggregates exhibit mass fractal-like behavior with a Hausdorf or mass fractal dimension, $D_f < 2$, even when the number of primary particles in an aggregate is small [3, 4, 10–21]. The mass fractal approximation implies the following relationship between the primary particle diameter, the number of primary particles in an aggregate and the radius of gyration of an aggregate [3]:

$$N = k_f (R_g/d_p)^{D_f}, \tag{1}$$

where k_f is a constant fractal prefactor and the aggregates are assumed to consist of monodisperse nonoverlapping spherical primary particles, i.e., the mean value of d_p is used in Eq. 1. This fractal-like behavior has important implications for the optical properties of soot which will be discussed next.

Measurements show that flame-generated soot ranges from small aggregates (dimensions on the order of 10 nm) near the start of soot formation, to large aggregates (dimensions on the order of 1 μm) emitted from large buoyant turbulent diffusion flames [3–21]. The larger-sized aggregates are too large for reasonable application of the Rayleigh scattering approximation and are too open structured for proper representation as equivalent compact spheres using the Mie scattering approximation [4]. These difficulties were established by direct measurements of soot scattering properties during early work [5–7]. For example, strong forward scattering was observed which is not representative of Rayleigh scattering behavior, while use of the Mie scattering approximation for an equivalent sphere still did not provide an adequate fit of scattering measurements [5–7]. The former behavior follows because the large soot aggregates in the size distribution dominate scattering properties and are too large to be approximated as Rayleigh scatter-

ing objects. Additionally, the fact that soot aggregates have fractal dimensions less than 2 implies that their structure is too open to be represented by a compact object such as an equivalent Mie scattering sphere [22]. The limitations of the Rayleigh and Mie scattering theories prompted subsequent development of optical theories of soot aggregates based on the Rayleigh–Debye–Gans (RDG) scattering approximation for mass fractal objects involving monodisperse spherical primary particles that just touch one another [3, 4, 11, 17]. The large refractive indices of soot raised questions about the validity of the RDG scattering approximation [4], however, recent work where both soot structure and scattering properties were known, has demonstrated performance of the RDG scattering theory for polydisperse fractal soot aggregates within experimental and computational uncertainties [20, 21, 23].

The reasonably successful evaluation of the RDG scattering theory for soot aggregates provides potential for resolving long-standing problems of the accurate determination of the refractive indices of soot [4, 24, 25], as well as for developing methods of solving the inverse problem so that soot structure properties can be found nonintrusively from scattering measurements [4, 20, 21, 24, 25]. Both these objectives, however, are inhibited by current limitations about the fractal and polydisperse properties of practical soot aggregates in flames. In particular, RDG theory requires values of R_g as a function of N but this determination is inhibited by current uncertainties concerning D_f and more particularly k_f [20, 21, 26]. Additionally, information about k_f requires analysis of actual three-dimensional soot aggregates, which can be facilitated by the availability of relationships between the projected and the actual properties of soot aggregates. Unfortunately, currently available information along these lines is rather limited. In particular, evaluation of relationships between projected and true three-dimensional properties of soot aggregates have only involved small aggregate samples and a few flame conditions [11, 12, 19]. Recent work by Sorensen and coworkers [24, 25] has sought to extend understanding of the projected and fractal properties of soot aggregates, but more development of their experimental methods will be needed for definitive results. Finally, Wu and Friedlander [26] address the fractal properties of aggregates based on existing results for numerically simulated populations of aggregates of spherical primary particles; however, the relevance of these findings to practical soot aggregates must still be established.

In view of current limitations about the structure and optical properties of soot aggregates, the objective of the present investigation was to study soot structure in order to define soot optical and fractal properties, as well as the relationships between actual and projected soot images. This work involved direct evaluation of the relationships between the number of primary particles and the projected image of an aggregate, the relationships between the radius of gyration of an aggregate and properties of its projected image, and the values of the Hausdorf or mass fractal dimensions and prefactors of soot in flame environments. The new information was developed by considering both numerically simulated and experimentally measured soot aggregates. The numerical simulations to create soot aggregates were based on cluster–cluster aggregation along the lines of Jullien and Botet [3], Mountain and Mulholland [13], and Farias et al. [23]. The experimental soot aggregates were obtained from two sources, as follows: the large soot aggregates found in the fuel-lean region of buoyant turbulent diffusion flames in the long residence time regime, where soot generation factors and soot structure are independent of flame position and residence time [19, 20, 27, 28]; and soot aggregates collected in both the fuel-rich and fuel-lean regions of laminar jet diffusion flames [29]. Taken together, the experimental soot properties involve a variety of fuels—acetylene, propylene, ethylene, and propane—burning in air within diffusion flames.

The paper begins with consideration of numerically simulated soot aggregates in order to establish relationships between actual and projected soot aggregate properties. Measured soot aggregate properties are then considered, emphasizing soot fractal properties.

NUMERICALLY SIMULATED AGGREGATES

Aggregate Simulation

Mountain and Mulholland [13] generated soot aggregates using a simulation involving cluster–cluster aggregation based on a solution of the Langevin equations. This approach yields fractal-like aggregates that satisfy the power-law relationship of Eq. 1 with $1.7 < D_f < 1.9$ and k_f ca. 5.5 for $N > 10$. However, a larger sample of aggregates was required for present work, and it was desired to have $1.7 < D_f < 1.8$ and k_f ca. 8.0 in order to correspond to recent experimental observations of the fractal properties of soot aggregates [19–21]. As a result, an alternative aggregate simulation, based on the approach used by Farias et al. [23], was used during the present investigation.

The present aggregate simulation involved creating a population of aggregates by cluster–cluster aggregation, following Jullien and Botet [3]. The simulation began with individual and pairs of primary particles which were attached to each other randomly, assuming uniform distributions of the point and orientation of attachment, while rejecting configurations where primary particles intersected. This procedure was continued in order to form progressively larger aggregates, but with the additional restriction that the aggregates should have $1.7 < D_f < 1.8$ with k_f of 8 for $N > 8$, based on Eq. 1 applied to the computed value of R_g for the aggregate. It was observed that D_f fell naturally in the range 1.6–1.9 for $N > 48$ during these simulations; therefore, few cluster-cluster combinations were rejected for inappropriate fractal properties when larger aggregates were constructed. Similarly, for D_f in the range 1.7–1.8, the value of k_f fell naturally near $k_f = 8.0$ for statistically significant populations of aggregates. Naturally, the numerically simulated aggregates were not useful for investigating aggregate fractal properties because their fractal properties had been prescribed. Nevertheless, these objects were useful for investigating relationships between projected and actual aggregate properties because the simulated aggregates were very similar to actual aggregates while their known geometry vastly simplified determinations of actual and projected aggregate properties.

The population of simulated aggregates involved N in the range 20–1000, considering 20 aggregate sizes. Results for each aggregate size were averaged over 20 different aggregates to yield a total sample of 400 aggregates. In order to fix ideas, a primary particle diameter of 50 nm was used for the simulations, which is typical of soot aggregates for heavily sooting materials [19]. Present results are normalized by d_p or A_p, however, and such normalized results are independent of d_p, at least for d_p less than 60 nm [20, 21].

Projected images of typical aggregates constructed using the present simulation are illustrated elsewhere for $N = 16$, 64, and 256 [23]. An example involving projected images of a given aggregate in three orthogonal directions for $N = 100$, is illustrated in Fig. 1. This partic-

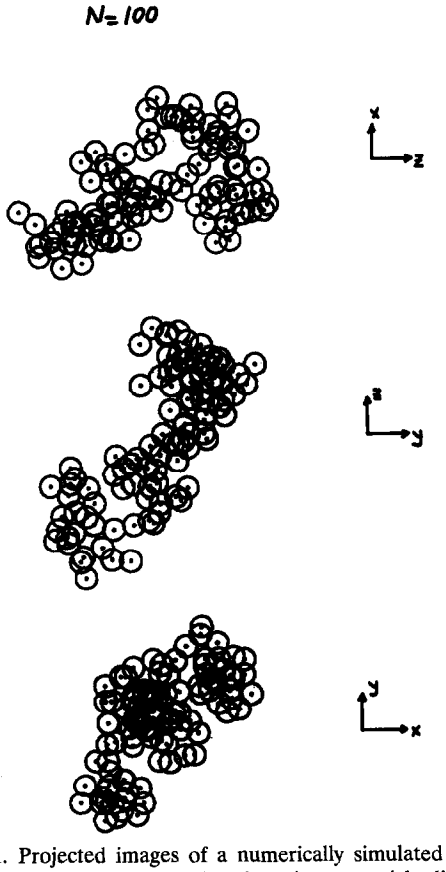

Fig. 1. Projected images of a numerically simulated soot aggregate. $N = 100$. Note that the primary particle diameter used in this simulation was 50 nm.

ular aggregate had $D_f = 1.76$ while $d_p = 50$ nm as noted earlier. Even though the value of N used in Fig. 1 is relatively modest, the dimensions of the aggregate are substantial, reaching maximum projected lengths greater than 1 μm. It is evident that the appearance of an aggregate varies considerably with the direction of the projection; it also varies substantially from aggregate to aggregate within a population of given size [23]. Nevertheless, the present simulated aggregates are qualitatively similar to both past experimental observations of soot aggregates [3, 6, 19–21] and other numerical simulations of soot aggregates [3, 13, 23]. Combined with their prescribed fractal properties, this behavior suggests that the present simulated aggregate populations are reasonably representative of the structure of soot aggregates found in flame environments.

Results and Discussion

The first property studied using the numerically simulated aggregates was the relationship between the number of primary particles in an aggregate and the projected area of the aggregate. Several workers have suggested the following relationship between the projected area of a soot aggregate, A_a, and N [12, 15–17, 19]:

$$N = k_a(A_a/A_p)^{\alpha}, \tag{2}$$

where α is an empirical projected area exponent and k_a is a constant normally taken to be unity. Results for the present simulated aggregates, based on random projections of the aggregates, are plotted according to Eq. 2 in Fig. 2. The power-law correlation of Eq. 2 is seen to provide an excellent fit of the data. The least-squares fit values of the correlation of Eq. 2 are $\alpha = 1.10$ and $k_a = 1.16$ with standard deviations of 0.002 and 0.01, respectively. The value of α is in reasonable agreement with earlier assessments although the present value of k_a exceeds the value of unity used in earlier work [12, 15–17, 19]. Further consideration of these differences will be undertaken when the experimental results are discussed.

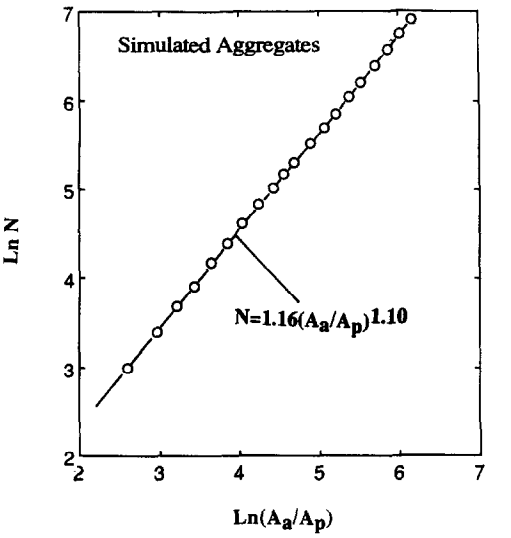

Fig. 2. Number of primary particles as a function of projected area ratio for simulated soot aggregates.

As noted earlier, the radius of gyration is an important aggregate property because it directly affects scattering properties computed using RDG theory. Thus, the simulated aggregates were used to compare actual values of the radius of gyration with values found from projected images of the aggregates. These results are illustrated in Fig. 3 where $R_g(3D)/R_g(2D)$ is plotted as a function of N for N in the range 20–1000. Remarkably, the ratio of the actual to projected radius of gyra-

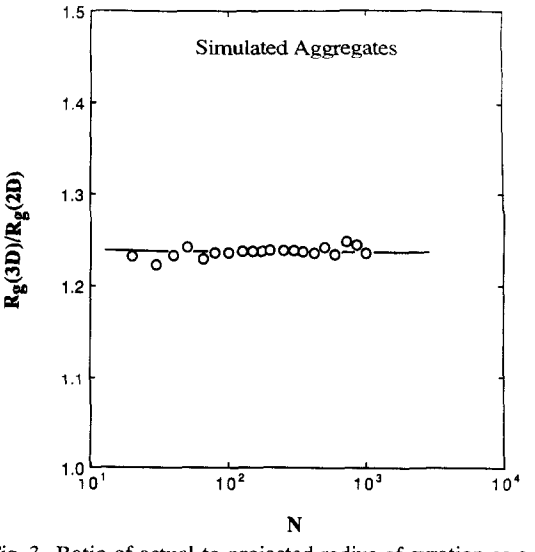

Fig. 3. Ratio of actual to projected radius of gyration as a function of aggregate size for simulated soot aggregates.

tion is essentially independent of N and has a value of 1.24 with a standard deviation less than 0.01, i.e.,

$$R_g(3D) = 1.24R_g(2D). \quad (3)$$

Thus, Eqs. 2 and 3 provide convenient relationships between the properties of projected images of aggregates, and the values of N and R_g needed to assess the fractal properties of aggregates that are defined in Eq. 1.

Direct evaluation of fractal properties from Eq. 1 requires either extensive data reduction of stereopair images or the alternative evaluation from the properties of projected images through Eqs. 2 and 3 that was just discussed. Information of this type is not often available so that several simplified methods based on projected aggregate dimensions have been developed, as discussed by Jullien and coworkers [3, 10]. One approach involves the use of the maximum projected length of the aggregate, L, as follows [3, 10]:

$$N = k_{fL}(L/d_p)^{D_f}. \quad (4)$$

An alternative approach, used during earlier work in this laboratory [19], involves use of the geometric mean of L, and the maximum projected width normal to L, W, as follows [3, 10]:

$$N = k_{fLW}\left((LW)^{1/2}/d_p\right)^{D_f}, \quad (5)$$

where the mean value of d_p is used in the correlations of Eqs. 4 and 5, similar to Eq. 1.

Comparing Eqs. 1, 4 and 5 indicates that L and $(LW)^{1/2}$ in Eqs. 4 and 5, act as surrogates for R_g in the fundamental fractal relationship of Eq. 1. Thus, the relationship between these various lengths is of interest and is illustrated in Fig. 4. These results involve plots of $L/(2R_g)$ and $(LW)^{1/2}/(2R_g)$ as a function of N. Unlike $R_g(3D)/R_g(2D)$, the ratios of either L or $(LW)^{1/2}$ and R_g are seen to decrease as N increases and only approach relatively constant values for $N > 100$, where

$$L/(2R_g) = 1.49, \quad (6)$$

$$(LW)^{1/2}/(2R_g) = 1.17, \quad (7)$$

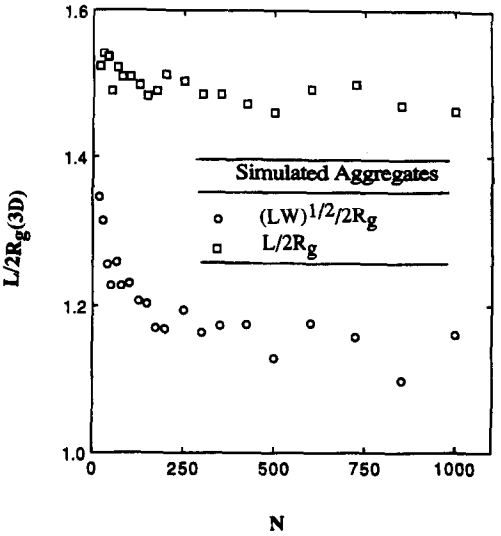

Fig. 4. Number of primary particles as a function of aggregate characteristic dimensions for simulated soot aggregates.

with standard deviations of 0.02 and 0.03, respectively. The smaller value of this ratio for $(LW)^{1/2}$ than for L is quite reasonable because $(LW)^{1/2}$ involves W, which is less than L by definition, for each aggregate. The effect of the variation of this ratio with N is of course negligible when data for large aggregates are processed to find D_f. However, this rarely is the case and the progressive reduction of the ratios generally acts to increase the apparent value of D_f when either L or $(LW)^{1/2}$ is used as a surrogate for R_g. Fortunately, the effect of this variation on determinations of D_f is not large, ca. 5%, as discussed subsequently in connection with experimental measurements of aggregate properties.

Puri et al. [18] also have considered values of $L/(2R_g)$ based on the measurements of Samson et al. [12]. These results were obtained using a 36-aggregate sample of overfire soot from a laminar acetylene flame and yield $L/(2R_g) = 1.78$ [18], which is roughly 20% larger than the present large N results. This behavior probably is caused by the relatively small aggregate sample used by Puri et al. [18], e.g., these results also exhibit an unusually small value of D_f as discussed later.

FLAME-GENERATED AGGREGATES

Experimental Methods

Soot structure also was observed using flame-generated aggregates collected by thermophoretic sampling. Sampling procedures were based on the methods of Dobbins and Megaridis [14–16] with specific techniques identical to past work in this laboratory [19]. The sampling surfaces were the carbon-supported copper grids used to hold TEM specimens (3-mm-diameter 200-mesh copper grids supported by a 20-nm-thick elemental carbon film, SPI Supplies, Philadelphia, part no. 3520C), aligned parallel to the mean flow direction. The probes were stored outside the flame and were inserted briefly into the flame environment using a double-acting pneumatic cylinder. Sampling times were controlled so that soot aggregates covered no more than 10% of the TEM grid in order to avoid overlapping aggregates on the grid. The time of transit of the grids to and from the sampling location through the flame environment was less than 5% of the sampling time so that soot on the grid was representative of the sampling location. This effect is not of any consequence for the soot sampled in the fuel-lean region of buoyant turbulent diffusion flames, however, because the properties of this soot are independent of position in any event [19].

The principles of thermophoretic sampling are discussed elsewhere [15–17, 30–32]. For present conditions, primary particle diameters were less than 60 nm, which implies that primary particle dimensions are smaller than the mean free path for all sampling conditions, so that the thermophoretic velocities of individual primary particles are identical. In addition, Rosner et al. [32] have shown that the thermophoretic velocities of aggregates and individual primary particles agree within 20%, even when the aggregates are larger than mean free path lengths. Thus, effects of intrinsic bias with respect to aggregate size for the present thermophoretic sampling technique are small.

The samples were observed using a JEOL 2000FX analytical electron microscope system with a 1-nm edge-to-edge resolution and sample tilting angles up to $\pm 45°$. Magnifications used for the present measurements were in the range 20,000–300,000. The procedure involved selecting aggregates randomly at low magnification, and then increasing the magnification in order to analyze them. The images were processed using the IMAGE computer algorithm to find projected aggregate areas and dimensions, as well as the projected positions and sizes of primary particles. Images at various angles of projection, as well as stereopairs, were then analyzed independently to find the corresponding three-dimensional properties of aggregates. Latex spheres having a diameter of 91 nm (with a standard deviation of 5.8 nm) were used to calibrate the TEM images. Specific sampling procedures and the experimental uncertainties of the soot structure parameters derived from these measurements will be considered when the results are discussed.

Typical TEM images of a soot aggregate found in the fuel-lean region of a buoyant turbulent ethylene/air diffusion flame are illustrated in Fig. 5. This particular aggregate has a primary particle diameter of 32 nm and contains 295 primary particles, based on observations at various angles of projection, which yields maximum projected dimensions of roughly 900 nm. The results shown in the photographs are for tilt angles of $-45°$, $0°$ and $45°$, which provides a means of locating each primary particle in space for absolute analysis of aggregate structure properties. Other properties of this aggregate are typical of earlier observations in the literature [8–21], as well as the numerically simulated aggregate of similar size illustrated in Fig. 1. In particular, the object is open-structured and consists of primary particles having a nearly constant diameter [4].

Results and Discussion: Turbulent Flames

The most extensive measurements of soot aggregate properties were made for the soot in the fuel-lean region of buoyant turbulent diffusion flames in the long residence time regime. As noted earlier, soot for a particular fuel at these conditions does not depend on position in the fuel-lean region or residence time [19].

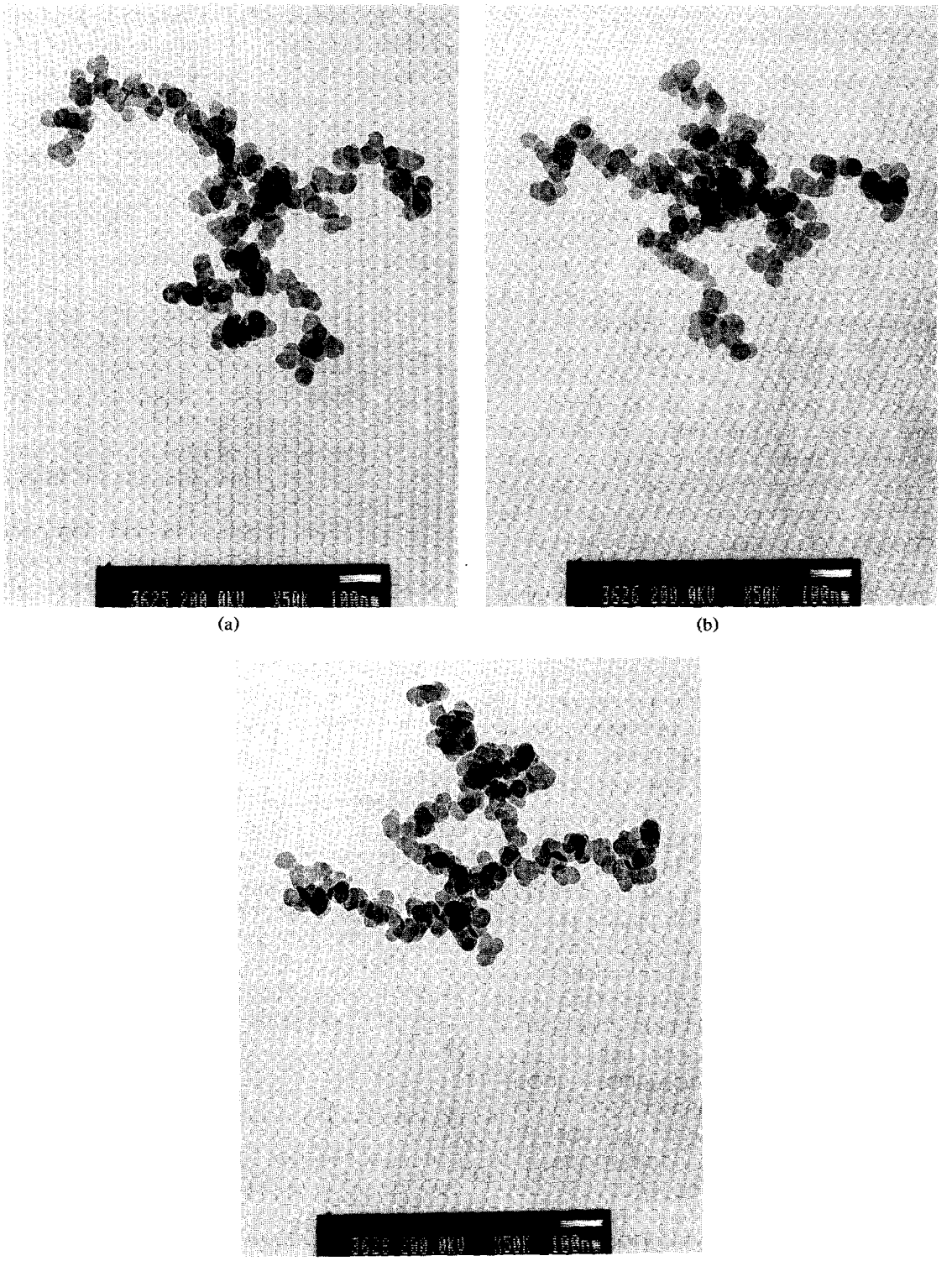

Fig. 5. TEM photographs of a typical soot aggregate from the fuel-lean region of a buoyant turbulent ethylene/air diffusion flame. Angles of projection (a) $-45°$, (b) $0°$, and (c) $45°$. Note, TEM length label is 100 nm long.

Specific measurements involved soot within acetylene, propylene, ethylene, and propane flames, see Ref. [19] for a complete description of experimental conditions. The measurements involved a total of 127 aggregates which contained 10–500 primary particles per aggregate.

The first issue to be considered using the measured aggregate structure properties was the relationship between the number of primary particles in an aggregate and its projected area on a TEM image. These results are illustrated in Fig. 6, for aggregates in the fuel-lean region of buoyant turbulent diffusion flames at long residence times. Composite results for soot from all the fuels are illustrated in Fig. 6. However, even though specific aggregate properties differ for the various flame systems, all the flames yield the same relationship between the number of primary particles in an aggregate and its projected area.

Similar to the simulated results illustrated in Fig. 2, the measured results illustrated in Fig. 6 suggest a correlation between the number of primary particles in an aggregate and its projected area. In fact, the empirical correlation found from the results illustrated in Fig. 6 is

$$N = 1.15(A_a/A_p)^{1.09}, \tag{8}$$

with standard deviations of α and k_a of 0.02 and 0.18, respectively. Within statistical significance, these values are identical to the results found for the numerically simulated aggregates which yielded $\alpha = 1.10$ and $k_a = 1.16$ with smaller standard deviations. Based on these findings it appears that the original correlation of Eq. 2 from Refs. 12, 15–17, and 19 is reasonable, except that k_a should be increased from unity to roughly 1.15. This effect implies that N was somewhat underestimated during earlier evaluations of fractal dimensions, based on expressions similar to Eqs. 4 and 5. This effect modifies values of k_{fL} and k_{fLW} inferred from these measurements but does not influence the determination of the fractal dimension, D_f.

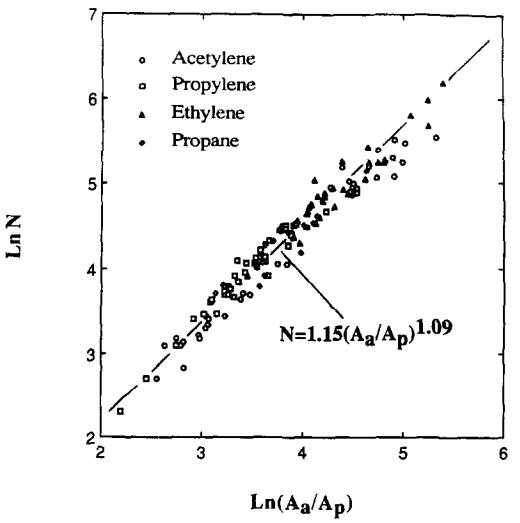

Fig. 6. Number of primary particles as a function of projected area ratio for soot aggregates from the overfire region of buoyant turbulent diffusion flames at long residence times.

The major effort of the present investigation was the determination of fractal prefactor, k_f, in Eq. 1 by measurements of N and R_g for the fuel-lean soot aggregates within buoyant turbulent diffusion flames in the long residence time regime. Similar to the results illustrated in Fig. 6, the fractal properties of aggregates for the various fuels—acetylene, propylene, ethylene and propane—were identical within experimental uncertainties, even though other properties—such as d_p and the mean number of primary particles per aggregate—differed considerably. The measured variation of N with R_g/d_p for the fuel-lean soot aggregates is illustrated in Fig. 7. The scatter of this data is appreciable, reflecting the problems of measuring R_g from projected images of aggregates at various angles. The fractal properties of the aggregates are clearly independent of fuel type, however, even though other properties of the aggregates (e.g., d_p, the mean number of primary particles per aggregate, etc.) differ considerably for soot formed from combustion of the various fuels. The best fit correlation of the measurements in Fig. 7 yields

$$N = 8.5(R_g/d_p)^{1.65}, \tag{9}$$

with standard deviations of D_f and k_f of 0.06 and 2.6, respectively. The standard deviation of k_f is relatively large; nevertheless, due to the relatively large data sample the corresponding uncertainty of the mean value of k_f is modest, i.e., the experimental uncertainty of the mean value of k_f (95% confidence) is 0.45 while the corresponding uncertainty of D_f is 0.12.

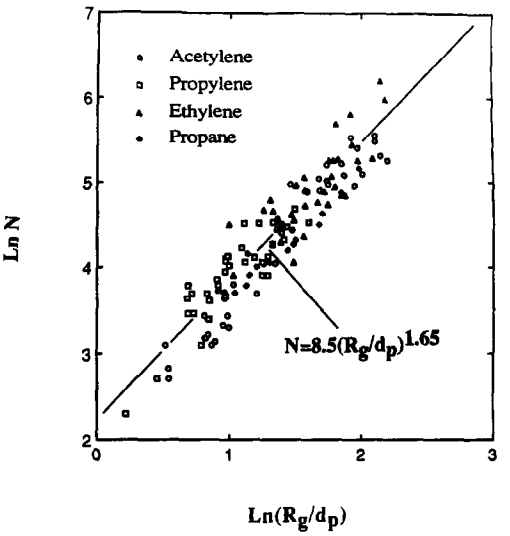

Fig. 7. Number of primary particles as a function of radius of gyration for soot aggregates from the overfire region of buoyant turbulent diffusion flames at long residence times.

The value of the fractal dimension found directly from the results of Fig. 7, $D_f = 1.65$, is somewhat low in comparison to earlier measurements of the same soot based on sampling and scattering determinations [19, 20]. For example, sampling and TEM measurements based on correlations of N as a function of $(LW)^{1/2}$ yielded $D_f = 1.75$ with an experimental uncertainty (95% confidence) of 0.07 over the four fuels [19]. The difference between the earlier and present values of D_f merits some explanation even though its statistical significance is marginal. This behavior follows from the discussion of Fig. 4; namely, that values of D_f based on $(LW)^{1/2}$ are somewhat larger than those based on R_g for a similar range of aggregate sizes, due to the progressive reduction of $(LW)^{1/2}/R_g$ with increasing aggregate size.

A more significant difference between the present value of D_f from Eq. 9, and other results, involves determinations of D_f based on light-scattering measurements [20]. For example, D_f found from the light-scattering measurements yielded a value of 1.82 with an experimental uncertainty (95% confidence) of 0.08 which is significantly greater than the present determination given by Eq. 9. This difference can be explained, however, by noting that the present sampling and TEM analysis yielded a progressive increase of D_f as both the size of largest aggregates and the sample size were increased. This behavior is consistent with larger observed values of D_f for the light-scattering measurements because these results emphasize the largest aggregates in the aggregate size distribution, as well, and clearly involve averages over a large number of aggregates [20]. Based on this observation, the effect of aggregate size on the present determination of D_f was estimated by Richardson extrapolation of the available variation of D_f with maximum aggregate size in the sample from the present data. This procedure involved plotting D_f found for samples containing aggregates smaller than a particular size N, as a function of $1/N$. The resulting plot was nearly linear for $N > 40$ and was extrapolated to $N \to \infty$ in order to obtain an estimate of $D_f = 1.83$ from the present sampling and TEM measurements [20]. Clearly, this value is in good agreement with the light-scattering determinations of $D_f = 1.82$, which also emphasize the largest aggregates in the distribution, as noted earlier.

The variation of k_f with maximum aggregate size in the present samples was less significant than the variation of D_f; therefore, $k_f = 8.5$ from Eq. 9 represents the present best estimate of this parameter. This value agrees within experimental uncertainties with recent estimates of Puri et al. [18] based on measurements of Samson et al. [12] and Megaridis and Dobbins [16]. In particular, analysis of measurements of N and R_g for a 36-aggregate sample of overfire soot from a laminar acetylene flame reported by Samson et al. [12] yielded $k_f = 9.22$ [18]. However, $D_f = 1.40$ for this sample, which is unusually low, so that the value of k_f was questioned based on potential sampling limitations [18]. Other estimates were obtained from measurements of Megaridis and Dobbins [16] for a nonsmoking laminar ethylene/air flame, taking $L/(2R_g) = 1.78$, to yield $k_f = 8.3$ and 8.9 for the two available aggregate samples from Ref. 16. As noted earlier, in connection with the discussion of Fig. 4, this value of $L/(2R_g)$ is somewhat larger than the present findings, although the corresponding values of k_f agree with present results within experimental uncertainties. Other earlier estimates of k_f are based on numerical

simulations of aggregation processes and generally yield values of k_f that are smaller than present estimates; see Wu and Freidlander [26] and references cited therein. An example of this behavior is $k_f = 5.8$, found by Puri et al. [18] based on the cluster-cluster aggregation simulation of Mountain and Mulholland [13]. The reasons for the low values of k_f from these simulations in comparison to subsequent measurements are not understood at the present time.

The fractal properties of the soot in the fuel-lean region of the buoyant turbulent diffusion flames at long residence times also can be considered from the results illustrated in Fig. 8. In this case, N is plotted as a function of the geometric mean projected aggregate size $(LW)^{1/2}$ for the four fuels over the same range of conditions as Fig. 7. The least-squares correlation of the measurements yields $D_f = 1.73$ and $k_{fLW} = 1.54$ with standard deviations of 0.04 and 0.30, respectively. As discussed in connection with Fig. 4, the apparent value of D_f is somewhat larger when found from $(LW)^{1/2}$, 1.73, than the value found from R_g, 1.65, for the same sample. All things considered, however, suggests the following estimates of the fractal properties of the fuel-lean soot: $D_f = 1.82$ with an uncertainty (95% confidence) of 0.08 from the light scattering measurements [20], supported by the extrapolated sampling results of Fig. 7; and $k_f = 8.5$ with an uncertainty (95% confidence) of 0.5, based on the sampling results of Fig. 7.

Results and Discussion: Laminar Flames

The final experimental results involved soot found in a laminar diffusion flame. In this case, samples were obtained at seven different locations along the axis of a weakly-buoyant acetylene/air laminar jet flame at a pressure of 0.25 atm. The test condition involved a burner diameter of 3.3 mm, and a burner exit Reynolds number of 80, which yielded a luminous soot-containing region roughly 50 mm long. Soot was sampled in both the fuel-rich and fuel-lean regions of the flame, over the range x/d of 1.92–13.42, to obtain a total of 618 aggregates with N in the range 5–1500.

The main results considered for soot in the laminar flame involved fractal properties. Measurements to find fractal properties are illustrated in Fig. 9, where N is plotted as a function of $(LW)^{1/2}$. Similar to results obtained from turbulent flames, the fractal properties of the soot illustrated in Fig. 9 were independent of the point where the soot was sampled, even though a range of fuel-lean and fuel-rich con-

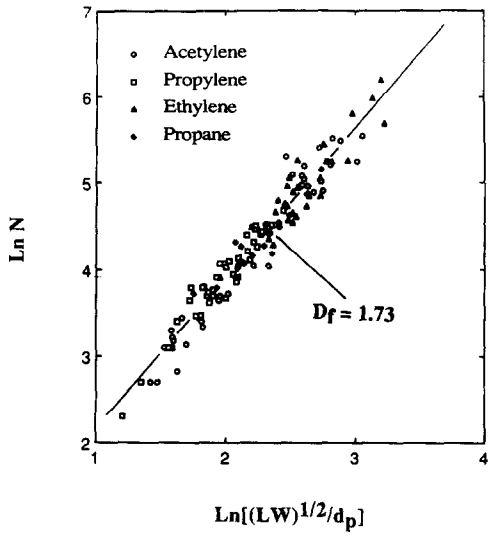

Fig. 8. Number of primary particles as a function of aggregate characteristic dimensions for soot aggregates from the overfire region of buoyant turbulent diffusion flames at long residence times.

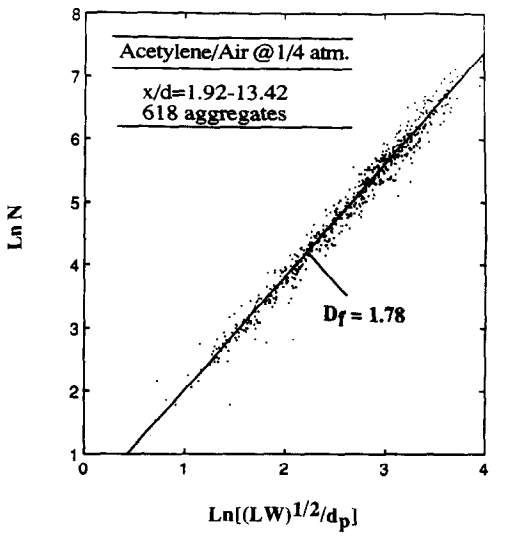

Fig. 9. Number of primary particles as a function of aggregate characteristic dimensions for soot aggregates from the underfire region of a laminar acetylene/air diffusion flame.

ditions were used and properties such as d_p and the mean number of primary particles per aggregate varied considerably with position in the flame. Then, treating all the laminar flame soot as a single sample population with respect to fractal properties yielded a best fit correlation of the measurements according to Eq. 5 with $D_f = 1.78$ and k_{fLW} of 1.33 with standard deviations of 0.012 and 0.23, respectively. The value of D_f for this soot is somewhat larger than the value for overfire soot found in Fig. 8 but this is felt to be due to the progressive increase of D_f with aggregate and sample size discussed in connection with Fig. 7, noting that both the sample size and the maximum value of N is larger for Fig. 9 than Fig. 8. Additionally, the difference between the results of Figs. 8 and 9 are relatively small so that properties of the laminar flame soot are identical to those of the soot within the fuel-lean region of buoyant turbulent diffusion flames at long residence times, within present experimental uncertainties. This finding suggests that the main fractal properties of soot, D_f and k_f, are relatively independent of the fuel and the flame condition.

CONCLUSIONS

Study of the structure of soot aggregates, considering aggregates obtained from numerical simulations using cluster–cluster aggregation, measured properties of soot aggregates from the fuel-lean region of buoyant turbulent diffusion flames at long residence times, and measured properties of soot aggregates from both the fuel-rich and fuel-lean regions of weakly buoyant laminar jet diffusion flames, yielded the following major conclusions:

1. In contrast to primary particle diameters and aggregate size, which vary considerably depending on flame conditions and fuel type, both the fractal properties, and the relationships between actual and projected soot aggregate structure properties, appear to be durable properties of soot that are relatively independent of fuel type and flame condition.
2. The best estimates of the fractal properties of soot aggregates based on present measurements yield $D_f = 1.82$ and $k_f = 8.5$ with experimental uncertainties (95% confidence) of 0.08 and 0.5, respectively. These results agree within experimental uncertainties with earlier determinations from sampling and TEM measurements [12, 16, 18–21].
3. Both computer simulations and experimental measurements indicated that it is possible to characterize soot aggregate structure properties from projected images, yielding $k_a = 1.15$, $\alpha = 1.09$ and $R_g(3D)/R_g(2D) = 1.24$, with standard deviations of these properties of 0.01, 0.002, and 0.01, respectively. The value of α is in good agreement with earlier estimates of this property [1, 15–17, 19]. In contrast, the present value of k_a is significantly larger than earlier estimates of unity for this parameter.
4. Values of the fractal dimension based on the geometric mean aggregate dimension, $(LW)^{1/2}$, were roughly 5% larger than values based on R_g for the aggregate samples considered here. This behavior is caused by a progressive reduction of $(LW)^{1/2}/R_g$ with increasing aggregate size. Additionally, values of D_f from sampling progressively increased as the sample size and the size of the largest aggregate were increased; in contrast, k_f exhibited a relatively small variation with sample and maximum aggregate size over the present range of conditions.

One of the authors (T.L.F.) would like to acknowledge scholarship support under the JNICT-CIENCIA BOLSAS Program (BD / 860 / 90-1B). Two of the authors (Ü.Ö.K and G.M.F.) would like to acknowledge support from the Building and Fire Research Laboratory of the National Institute of Standards and Technology (Grant No. 60NANB1D1175), the Microgravity Combustion Science Program of NASA (Contract No. NAG3-1245), and the Office of Naval Research (Grant No. N00014-93-1-0321). The collaboration between Instituto Superior Técnico and The University of Michigan is sponsored by AGARD, Support Project P-101. The assistance of Tienmin Chu with the TEM measurements is also gratefully acknowledged.

REFERENCES

1. Tien, C. L., and Lee, S. C., *Prog. Energy Combust. Sci.* 8:41–59 (1982).

2. Viskanta, R., and Mengüc, M. P., *Prog. Energy Combust. Sci.* 13:97–160 (1987).
3. Jullien, R., and Botet, R., *Aggregation and Fractal Aggregates*, World Scientific Publishing Co., Singapore, 1987.
4. Köylü, Ü. Ö., and Faeth, G. M., *J. Heat Transf.* 115:409–417 (1993).
5. Erickson, W. D., Williams, G. C., and Hottel, H. C., *Combust. Flame* 8:127–132 (1964).
6. Dalzell, W. H., Williams, G. C., and Hottel, H. C., *Combust. Flame* 14:161–170 (1970).
7. Wersborg, B. L., Howard, J. B., and Williams, G. C., *Fourteenth Symposium (International) on Combustion*, The Combustion Institute, Pittsburgh, 1972, p. 929.
8. Medalia, A. I., and Heckman, F. A., *Carbon* 7:567–582 (1969).
9. Magnussen, B. F., *Fifteenth Symposium (International) on Combustion*, The Combustion Institute, Pittsburgh, 1974, p. 1415.
10. Tence, M., Chevalier, J. P., and Jullien, R., *J. Physi. (Paris)* 47:1989–1998 (1986).
11. Martin, J. E., and Hurd, A. J., *J. Appl. Cryst.* 20:61–78 (1987).
12. Samson, R. J., Mulholland, G. W., and Gentry, J. W., *Langmuir* 3:272–281 (1987).
13. Mountain, R. D., and Mulholland, G. W., *Langmuir* 4:1321–1326 (1988).
14. Dobbins, R. A., and Megaridis, C. M., *Langmuir* 3:254–259 (1987).
15. Megaridis, C. M., and Dobbins, R. A., *Combust. Sci. Technol.* 66:1–16 (1989).
16. Megaridis, C. M., and Dobbins, R. A., *Combust. Sci. Technol.* 71:95–109 (1990).
17. Dobbins, R. A., and Megaridis, C. M., *Appl. Opt.* 30:4747–4754 (1991).
18. Puri, R., Richardson, T. F., Santoro, R. J., and Dobbins, R. A., *Combust. Flame* 92:320–333 (1993).
19. Köylü, Ü. Ö., and Faeth, G. M., *Combust. Flame* 89:140–156 (1992).
20. Köylü, Ü, Ö., and Faeth, G. M., *J. Heat Transf.*, 116:152–159 (1994).
21. Köylü, Ü. Ö., and Faeth, G. M., *J. Heat Transf.*, in press.
22. Berry, M. V., and Percival, I. C., *Optica Acta* 33:577–591 (1986).
23. Farias, T., Carvalho, M. G., Köylü, Ü. Ö., and Faeth, G. M., *J. Heat Transf.*, in press.
24. Sorensen, C. M., Cai, J., and Lu, N., *Appl. Opt.* 31:6547–6557 (1992).
25. Cai, J., Lu, N., and Sorensen, C. M., *Langmuir* 9:2861 (1993).
26. Wu, M. K., and Friedlander, S. K., *J. Colloid Inter. Sci.* 159: 246–248 (1993).
27. Sivathanu, Y. R., and Faeth, G. M., *Combust. Flame* 81:133–149 (1990).
28. Köylü, Ü. Ö., and Faeth, G. M., *Combust. Flame* 87:61–76 (1991).
29. Sunderland, P. B., Köylü, Ü. Ö., and Faeth, G. M., *Combust. Flame*, in press.
30. Hinds, W. C., *Aerosol Technology*, Wiley, New York, 1982, pp. 83, 154.
31. Eisner, A. D., and Rosner, D. E., *Combust. Flame* 6:153–166 (1985).
32. Rosner, D. E., Mackowski, D. W., and Garcia-Ybarra, P., *Combust. Sci. Technol.* 80:87–101 (1991).

Received 28 January 1994; revised 7 June 1994